Firas A. Khasawneh[1]
Department of Engineering Mathematics,
University of Bristol,
Bristol, BS8 1TR, United Kingdom
e-mail: firas.khasawneh@bristol.ac.uk

Oleg A. Bobrenkov
Department of Mechanical and
Aerospace Engineering,
New Mexico State University,
Las Cruces, NM 88003

Brian P. Mann
Department of Mechanical Engineering and
Materials Science,
Duke University,
Durham, NC 27708

Eric A. Butcher
Department of Mechanical and
Aerospace Engineering,
New Mexico State University,
Las Cruces, NM 88003

Investigation of Period-Doubling Islands in Milling With Simultaneously Engaged Helical Flutes

This paper investigates the stability of a milling process with simultaneously engaged flutes using the state-space TFEA and Chebyshev collocation methods. In contrast to prior works, multiple flute engagement due to both the high depth of cut and high step-over distance are considered. A particular outcome of this study is the demonstration of a different stability behavior in comparison to prior works. To elaborate, period-doubling regions are shown to appear at relatively high radial immersions when multiple flutes with either a zero or nonzero helix angle are simultaneously cutting. We also demonstrate stability differences that arise due to the parity in the number of flutes, especially at full radial immersion. In addition, we study other features induced by helical tools such as the waviness of the Hopf lobes, the sensitivity of the period-doubling islands to the radial immersion, as along with the orientation of the islands with respect to the Hopf lobes.
[DOI: 10.1115/1.4005022]

Keywords: milling, temporal finite element, Chebyshev, stability, helical flutes

1 Introduction

Self-excited vibrations can occur when the forces exciting a system are coupled to the state variables. This coupling can be the result of a feedback mechanism where the excitation forces are a function of current and past state variables. The equations of motion incorporating such mechanism are typically delay differential equations (DDEs) which are either autonomous or time-varying. One physical application for DDEs is found in metal removal processes. More specifically, many studies have investigated the occurrence of self-excited vibrations in machining, commonly known as chatter.

Chatter is typically characterized by large amplitude oscillations that deteriorate the surface finish and can also damage the tool, machine spindle, and the workpiece. For a limited class of DDEs, e.g., continuous turning, the stability boundaries can be obtained in a closed form [1]. However, the stability analysis of more general DDEs requires using approximation techniques, such as semidiscretization [2], Chebyshev-based methods [3–5], collocation methods [6], temporal finite element analysis (TFEA) [7–10], and frequency domain techniques [11,12]. Numerical simulation is also used to study machining stability [13–16]; however, analytical and/or semianalytical predictions of stability can quickly and accurately give stability regions over the process parameter space of interest, making them superior to tedious numerical simulations [17–20].

The presence of piecewise continuous coefficients in the DDE considerably increases the level of complexity. Milling, for instance, is a common metal removal process which is commonly approximated as a periodic, piecewise, continuous system. Therefore, approximation schemes, such as TFEA [9,10,21–24] and collocation methods [25,26], are typically necessary to determine milling stability. The stability of milling processes is typically reported through stability diagrams which chart the boundaries between stable and unstable cuts as a function of the spindle speed and depth of cut [27–29]. A milling process is stable if it is chatter-free, whereas at the onset of chatter, the process becomes unstable. These diagrams enhance efficiency and reduce costs by eliminating the need for trial and error. In addition to solving for the system stability, semianalytical techniques can determine the type of bifurcation associated with instabilities.

For example, recent studies have shown that a new bifurcation phenomena can occur in highly intermittent cutting. Besides Neimark-Sacker or secondary Hopf bifurcations, period-doubling bifurcations have been analytically predicted in Refs. [16,18,30,31] and confirmed experimentally in Refs. [22,32,34]; a specific outcome from these works was that they found period-doubling at low radial immersions when only a single tooth was cutting.

A different stability behavior for helical mills was reported and experimentally verified in Refs. [10,30,35–37]. Closed boundaries, or islands, of unstable period-doubling were shown to appear in the stability diagram due to the helical flutes of the tool. In these works, the period-doubling islands were shown only at relatively low radial immersions. Furthermore, Refs. [10,37] studied the case of only one flute cutting at a time, see Fig. 1(*a*), whereas Refs. [35,36] investigated the case of multiple flutes simultaneously cutting when using a high depth of cut, see Fig. 1(*b*). Reference [26] studied the case of multiple engaged flutes with a zero-helix angle; however, the stability analysis for the cases of multiple nonzero helix flutes simultaneously cutting due to a high step-over distance, (see Fig. 1(*c*)), or due to a combination of a high depth of cut and a high step-over distance, see Fig. 1(*d*), has not received much attention.

In this paper, the state-space TFEA method and the Chebyshev collocation approach are used to study the stability of a milling process. The added complexity of simultaneously engaged flutes for both zero- and nonzero helix tools is considered. In contrast to prior works, multiple flute engagement due to both the high depth of cut and high step-over distance are investigated. A particular outcome of this study is the demonstration of a different stability behavior at the loss of stability in comparison to prior results. To elaborate, period-doubling regions are shown to appear at relatively high radial immersions when multiple flutes with either a zero or nonzero-helix angle are simultaneously cutting. We also elucidate the sensitivity of the period-doubling regions to the radial immersion and reveal the strong influence of the parity in the

[1]Corresponding author.

Contributed by the Technical Committee on Vibration and Sound of ASME for publication in the JOURNAL OF VIBRATION AND ACOUSTICS. Manuscript received July 16, 2010; final manuscript received July 14, 2011; published online January 18, 2012. Assoc. Editor: Steven W. Shaw.

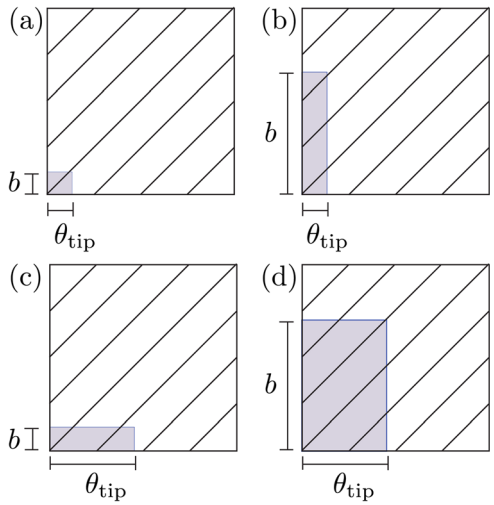

Fig. 1 The different cases associated with a helical milling tool. The gray area represents the cutting zone and, in graph (*a*) only a single flute is cutting at any instant, while in graphs (*b*) and (*c*) multiple flutes are cutting due to a high depth of cut, and a high radial step-over distance, respectively. Graph (*d*) shows the case of a high depth of cut combined with a high radial step-over distance. The variables shown in the figure are defined in Sec. 2.

number of flutes, especially at full radial immersion, on the stability behavior. We also present upmilling stability charts where, in contrast to typical results in milling literature, the helical tools induce a strong waviness along the depth of cut direction in the Hopf lobes.

2 Mechanical Model

The equation of motion for a single-mode helical mill compliant only in the y direction, such as the one shown in Fig. 2, (or similarly, for a workpiece compliant in the y direction), is described by

$$\ddot{y}(t) + 2\zeta\omega_{\text{n}}\dot{y}(t) + \omega_{\text{n}}^2 y(t) = \frac{1}{m_y}F_y(z,t,\tau) \tag{1}$$

where m_y, ω_{n}, and ζ are the modal mass, natural frequency, and damping ratio, respectively. The term $F_y(z,t,\tau)$ describes the cutting forces in the y direction while the time delay $\tau = 2\pi/N\Omega$ is the tooth passage period for an N-tooth cutter rotating at a spindle speed Ω (rad/s). An analytical expression for F_y can be obtained by first introducing the differential forces, shown in Fig. 3, in the tangential and radial directions [38] according to

$$dF_t = K_t w(\theta_n(t,z),\tau)dz \tag{2a}$$

$$dF_r = K_r w(\theta_n(t,z),\tau)dz \tag{2b}$$

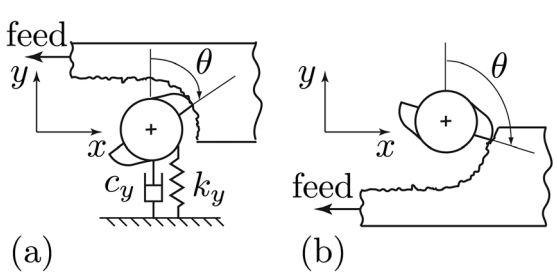

Fig. 2 Illustrations of (*a*) upmilling, and (*b*) downmilling

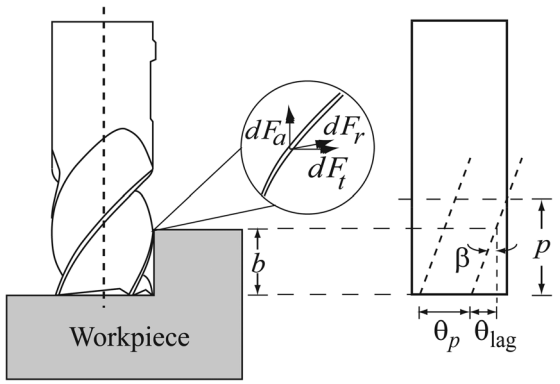

Fig. 3 Schematic of a helical end mill with multiple flutes and the differential cutting forces in the axial, radial, and tangential directions

where K_t and K_r are the tangential and radial specific cutting force coefficients, respectively, and the variable z varies along the axial direction of the tool from 0 at the tip to b which is the depth of the cut. The angle $\theta_n(t,z)$ describes the rotation angle of the nth flute from the vertical reference shown in Fig. 2, and is described by

$$\theta_n(t,z) = \Omega t - (n-1)\theta_{\text{p}} - \kappa z \tag{3}$$

where $n = 1,2,\ldots,N$, θ_{p} is the tool pitch angle, i.e., $\theta_{\text{p}} = 2\pi/N$ for a tool with uniformly spaced flutes, and $\kappa = 2\tan\beta/D$ is a helix parameter. The radial chip thickness for the reference cutting tooth can be found by applying the circular tool path assumption which yields [39,40]

$$w(\theta_n(t,z)) = h\sin(\theta_n(t,z)) + [y(t) - y(t-\tau)]\cos(\theta_n(t,z)) \tag{4}$$

where h is the feed per tooth. The total force in the y direction is found by integrating Eqs. (2*a*) and (2*b*) with respect to the differential axial depth dz which yields

$$F_y = g_n(t)\int_{z_a(n,t)}^{z_b(n,t)}\left[\frac{dF_t}{dz}\sin\theta_n(t,z) - \frac{dF_r}{dz}\cos\theta_n(t,z)\right]dz \tag{5}$$

where $g_n(t)$ is a switching function: its value is 1 if the nth tooth is cutting, and 0 if the tooth exits the cut. The functions $z_a(n,t)$ and $z_b(n,t)$ describe the lower and upper limits of integration, respectively, and they are graphed in Fig. 4 where they are shown to vary according to

$$z_a(n,t) = \begin{cases} 0 & \text{if} \quad \theta_{\text{st}} \le \theta_n \le \theta_{\text{st}} + \theta_{\text{tip}} \\ \dfrac{\theta_n - (\theta_{\text{st}} + \theta_{\text{tip}})}{\kappa} & \text{if} \quad \theta_{\text{st}} + \theta_{\text{tip}} < \theta_n \end{cases} \tag{6a}$$

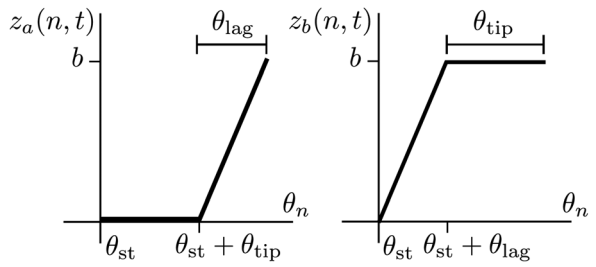

Fig. 4 A plot of the integration limits described in Eqs. (6) as a function of the flute rotation angle

$$z_b(n,t) = \begin{cases} \dfrac{\theta_n - \theta_{st}}{\kappa} & \text{if} \quad \theta_{st} \le \theta_n \le \theta_{st} + \theta_{lag}, \\ b & \text{if} \quad \theta_{st} + \theta_{lag} < \theta_n, \end{cases} \tag{6b}$$

where θ_{tip} is the angular distance over which the tool is cutting at $z = 0$, θ_{st} is the entry angle which is 0 for upmilling and $\pi - \theta_{tip}$ for downmilling, while $\theta_{lag} = \kappa b$ is the angular distance defined in Fig. 3.

The angular distance θ_{tip} depends on the ratio of the radial step-over distance to the tool diameter, which is often called the radial immersion (RI), according to

$$\theta_{tip} = \cos^{-1}(1 - 2\text{RI}) \tag{7}$$

Substituting the expression for the total force in the y direction, Eq. (5), into Eq. (1), the equation of motion now reads

$$\ddot{y}(t) + 2\zeta\omega_n\dot{y}(t) + \omega_n^2 y(t) = \frac{K_c(t,b)}{m_y}(y(t) - y(t-\tau)) \tag{8}$$

where only the dynamic chip thickness was considered, i.e., by ignoring the term $h \sin\theta_n(t,z)$ in Eq. (4) which does not affect the stability analysis. The directional force coefficient $K_c(t,b)$ is τ-periodic and is a function of time and the depth of cut b [36,37]. This coefficient is defined using Eqs. (2*a*), (2*b*), and (4) as follows

$$K_c(t,b) = \sum_{n=1}^{N_t} g_n(t) \int_{z_a(n,t)}^{z_b(n,t)} (K_t \sin\theta_n \cos\theta_n - K_r \cos^2\theta_n) dz \tag{9}$$

where the summation is over the total number of simultaneously engaged flutes $N_t = \lceil (\theta_{tip} + \theta_{lag})/\theta_p \rceil$, where $\lceil \cdot \rceil$ is the ceiling function.

It is necessary here to make a distinction between the tool pitch angle θ_p and the mill helix pitch p which are related according to $\theta_p = \kappa p$. Whereas the pitch angle describes the angular distance between two consecutive teeth, the mill helix pitch describes the distance between two adjacent flutes along the axis of the tool, as shown in Fig. 3. Furthermore, the mill helix pitch is a geometric property of helixes, and it is given mathematically by [35]

$$p = \frac{D\pi}{N \tan\beta} \tag{10}$$

where D is the diameter of the tool and β is the helix angle defined in Fig. 3. Both θ_p and p play an important role in determining whether multiple flutes are cutting or not. Specifically, the condition for multiple flutes in contact is

$$\lceil (\theta_{tip} + \theta_{lag})/\theta_p \rceil > 1 \tag{11}$$

This condition captures cases (*b*), (*c*) and (*d*) in Fig. 1.

In order to use the state-space TFEA method or the Chebyshev collocation approach, Eq. (8) is first re-written in its state-space form

$$\frac{d\mathbf{y}(\mathbf{t})}{dt} = \mathbf{A}(t)\mathbf{y}(t) + \mathbf{B}(t)\mathbf{y}(t-\tau) \tag{12}$$

where $\mathbf{A}(t+T) = \mathbf{A}(t)$ and $\mathbf{B}(t+T) = \mathbf{B}(t)$ are time-periodic with the period T equal to the time delay, τ.

The state-space TFEA method [41–43] or the Chebyshev collocation method [25,26] can then be used to transform Eq. (12) into a dynamic map of the form

$$\mathbf{y}_{n+1} = \mathbf{U}\mathbf{y}_n \tag{13}$$

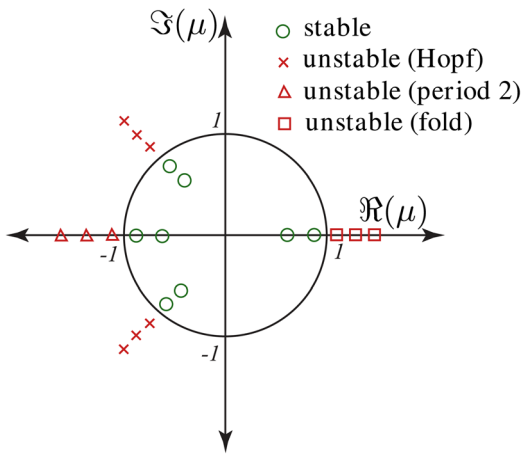

Fig. 5 The stability criteria dictates that all the eigenvalues μ of the monodromy operator U should lie within the unit circle in the complex plane. Moreover, the manner in which the eigenvalues depart the unit circle produces different bifurcation behavior. For example, an eigenvalue leaving the unit circle through −1 or 1 results in a period-doubling bifurcation or a fold bifurcation, respectively, whereas two complex conjugate eigenvalues departing the unit circle result in a secondary Hopf bifurcation.

where **U** is a finite dimensional approximation of the infinite dimensional monodromy operator for time-periodic DDEs. Equation (8) represents a discrete solution form for Eq. (8) that maps the states of the system over one delay period τ. The eigenvalues of **U** determine the asymptotic stability of the DDE according to the condition shown in Fig. 5.

3. Discussion

The results from the stability analysis for the milling process, described by Eq. (12), are given in this section. The cases studied are for multiflute cutters with zero- and nonzero helix angles. Both upmilling and downmilling cases were investigated using the state-space TFEA and Chebyshev collocation methods. The two analysis techniques produced identical stability charts; hence, we only show one set of converged stability charts for each case study. The interest here is in the unstable period-doubling islands that appear in the stability diagrams when using helical flutes.

Note that the zero-helix case can also produce period-doubling islands; however, these islands appear due to the parametric nature of the forces in milling and not due to the helix angle. The islands that appear in the zero-helix case are called parametrically induced islands whereas the islands associated with the helical tool are called helix-induced islands [35,44]. Figure 6 shows an example of a parametrically induced island for downmilling with a 3-flute cutter at 0.05 radial immersion. The stability of several points was found using the TFEA approach and is noted on the stability chart using the notation of Fig. 5. The dots denote stable regions whereas triangles denote an unstable period-doubling region. Since we are primarily interested in the island phenomena associated with helical mills, the zero-helix cases are only given for reference.

The parameters used to obtain the stability plots in this study were introduced in Refs. [35,36] and are shown in Table 1. The results for downmilling are shown in Figs. 7 and 8, whereas upmilling results are shown in Fig. 10. For the downmilling results, both a zero-helix mill (light line), and a helical mill with $\beta = 30°$ (dark line) are reported in each diagram. The horizontal dotted line in each figure marks the helix pitch and the type of bifurcation is also marked on each lobe with "H" indicating a Hopf bifurcation, and

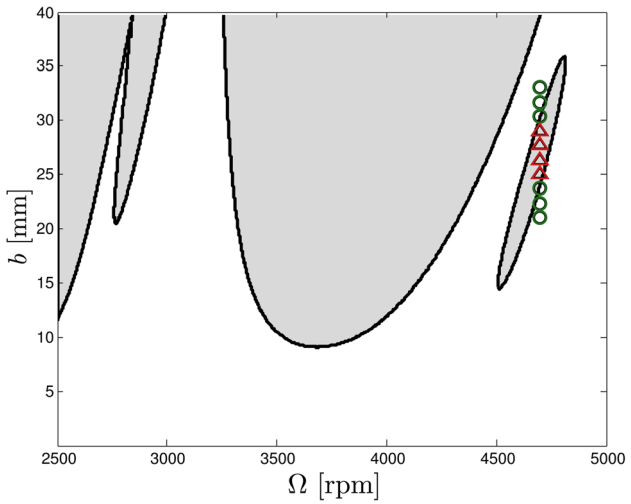

Fig. 6 A parametrically induced period-doubling island appears when downmilling at 0.05 radial immersion with a zero-helix 3-flute cutter. The stability of several points is also noted using a notation consistent with the one used in Fig. 5; circles were used to denote a stable region, whereas triangles were used to denote unstable period-doubling regions.

"P" indicating period-doubling lobes. The authors acknowledge that changing the geometry of the tool would, in general, change the specific cutting coefficients K_r and K_t. Therefore, a one-to-one stability comparison between a zero-helix tool and a helical one would require accounting for these changes.

Table 1 The parameters used to generate the stability plots in this study

m (Kg)	ω_n (Hz)	ζ	K_t (N/mm^2)	K_r (N/mm^2)
5.364	319.375	0.0196	804.3	331

In Fig. 7, a radial immersion of 0.05 and $N = 4$ produced identical results to those obtained through a frequency domain stability analysis in Ref. [36]. This case corresponds to graphs (*a*) and (*b*) in Fig. 1, where incrementing the depth of cut to higher values, i.e., higher than helix pitch p, results in multiple-flute engagement (see Fig. 1(*b*)). It can be seen that the period-doubling boundary which corresponds to the zero-helix case transforms into closed, bounded regions of period-doubling that are often called islands. The depths of cut in the period-doubling free zones between any two islands correspond to the integer multiples of the helix pitch. This is because at these values of cutting depths the helical flutes average the time-periodic forces and the system becomes autonomous [35].

The period-doubling islands for the 4-flute cutter still appeared as the radial immersion was increased to 0.25 and 0.50 in the first column of Fig. 7; the latter is the borderline case for only one flute in the cut when using a zero-helix mill and 4 cutting flutes. The period-doubling lobes for the zero-helix case and the islands for the helical tool case were still apparent at these radial immersions. However, in contrast to prior works on a single flute in the cut for cutters with more than 2 flutes, a further increase in the radial immersion in the first column of Fig. 7 to 0.75 causes multiple flute engagement for the zero-helix case and produces cases similar to those depicted in Figs. 1(*c*) and 1(*d*) for the helical tool with

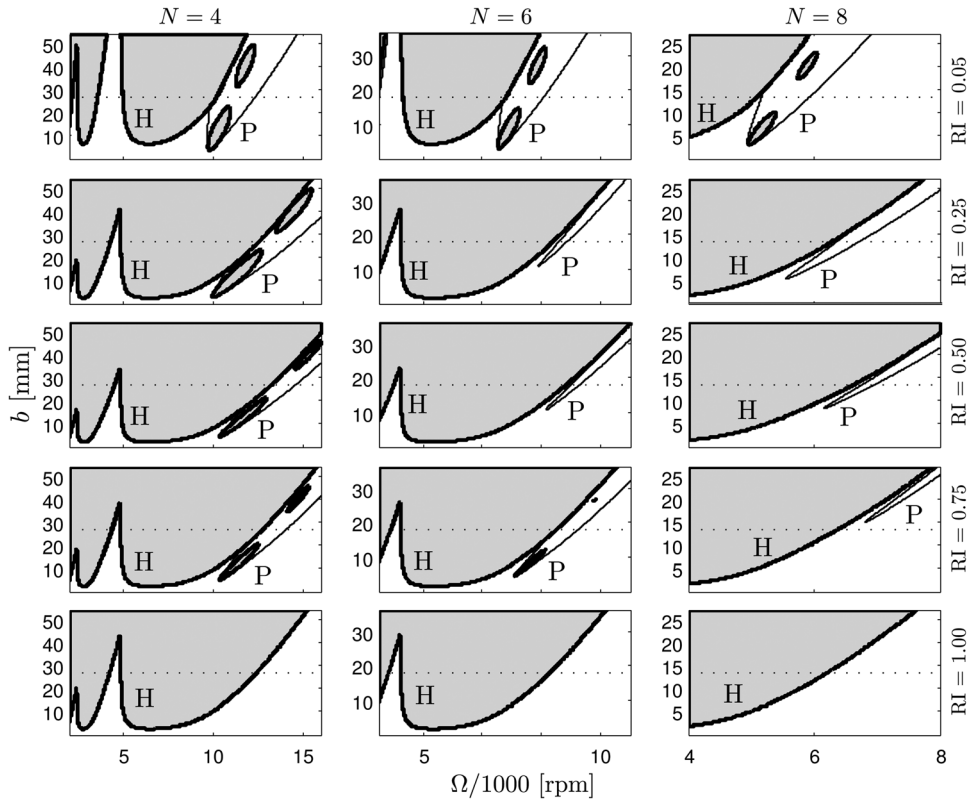

Fig. 7 Downmilling stability diagrams of Eq. (8) for cutters with 4, 6, and 8 flutes. The light line represents the zero-helix case while the thick line represents a helical tool with $\beta = 30°$. The parameters used to generate the plots are shown in Table 1 and the radial immersions used are (*a*) 0.05, (*b*) 0.50, (*c*) 0.75, and (*d*) 1.0. "H" indicates Hopf bifurcations, while "P" indicates period-doubling bifurcations.

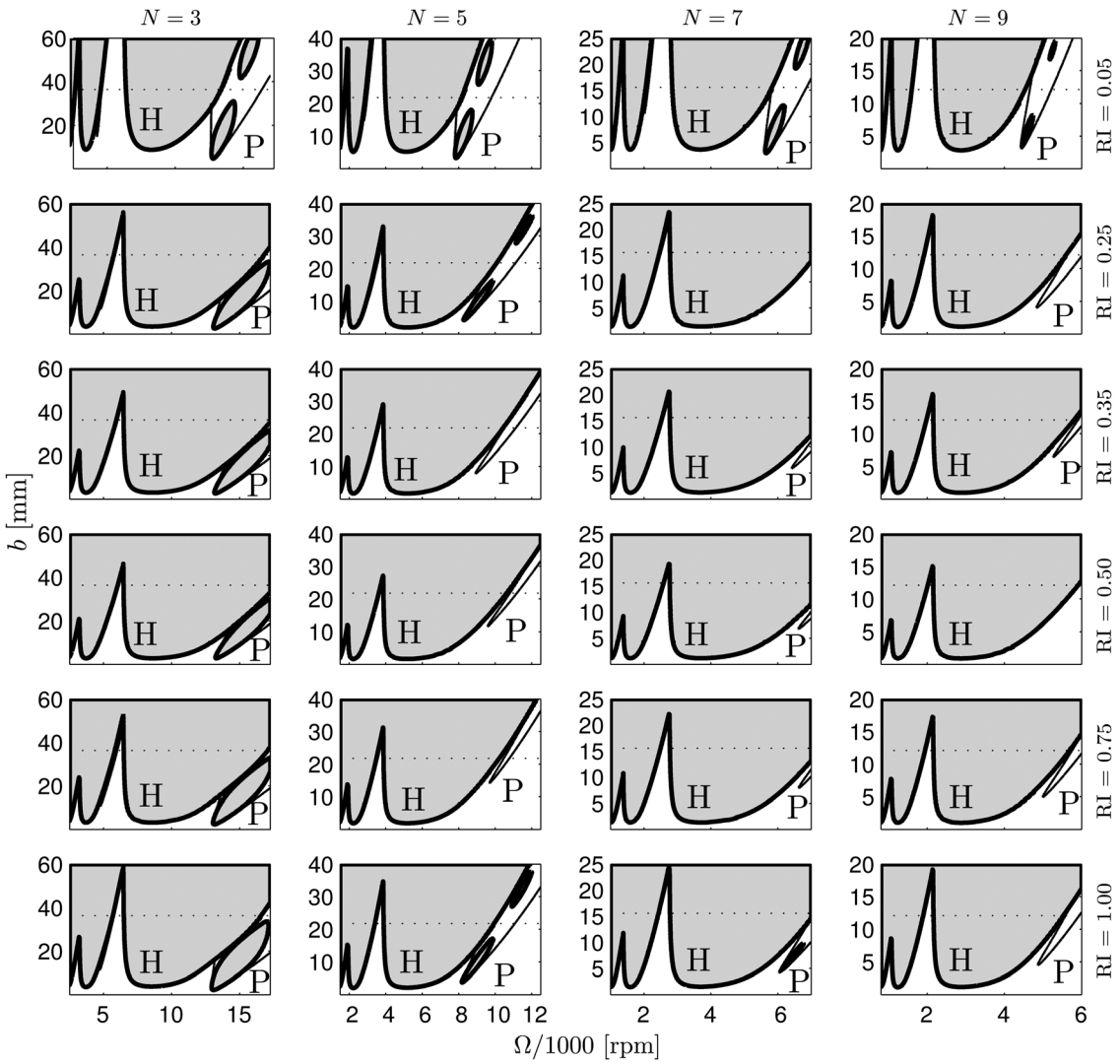

Fig. 8 Downmilling stability diagrams for cutters with $\beta = 30^\circ$ and various odd number of flutes at various radial immersion levels

4 flutes. The appearance of period-doubling lobes at this relatively high radial immersion diverges from the stability behavior for a single engaged flute. The period-doubling regions disappear at full radial immersion (see the last row of Fig. 7), and the results for zero-helix and helical tools become identical under the assumption of constant specific cutting coefficients.

The case for a 6-flute cutter demonstrated a different behavior, as shown in Fig. 7. For example, in Fig. 7 for a 6-flute cutter, period-doubling regions still appeared for the zero-helix case when only one flute was cutting, i.e., at RI = 0.05 and RI = 0.25, along with the cases with higher radial immersions and a zero-helix mill in the subsequent rows (except at RI = 1.00). However, when a helical mill was used, the period-doubling lobes disappeared and only Hopf lobes persisted for RI = 0.25 and 0.50. Nevertheless, period-doubling lobes reappeared as the radial immersion was increased to 0.75. This shows the sensitivity of the period-doubling islands to changes in the radial immersion and emphasizes the importance of predicting their reappearance even at higher radial immersions.

In contrast, for an 8-flute cutter, whereas period-doubling lobes appeared for the zero-helix case, only Hopf lobes appeared for the helical tool cases. This is due to the fact that as the number of teeth is increased, the spacing between the helical flutes gets smaller, decreasing both the pitch angle and the helix pitch. The forces are therefore averaged out around the tool helix over the full range of cutting speeds and depths of cut. The smoothing effect of the helix angle transforms a discontinuous milling process into a continuous one as the number of flutes is increased. Hence, when a sufficient number of cutting edges is used, only the main Hopf instability region appears.

One common feature of all the cases, shown in Fig. 7, is the absence of period-doubling regions at full radial immersion (RI = 1.00). At this value of radial immersion only Hopf lobes appear and the stability diagram for zero-helix and helical flutes become almost identical for cutters with an even number of flutes. However, a different effect was revealed when cutters with an odd number of flutes were studied.

For example, Fig. 8 shows the downmilling stability charts for several combinations of radial immersions and various cutters with an odd number of flutes. It can be seen that at full radial immersion, all of the studied cases showed an area of period-doubling for the zero-helix case. Furthermore, all of the cases except for the 9-flute cutter resulted in period-doubling islands at full radial immersion. This influence of the parity in the number of flutes on stability at full radial immersion has important practical implications: not only the depth of cut, radial immersion, and the helix angle need to be optimized in milling, but also the parity of the number of flutes needs to be considered. An even number

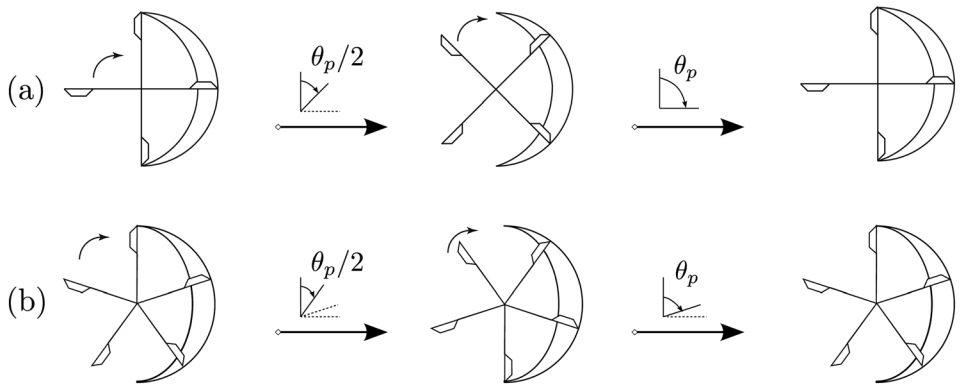

Fig. 9 Snapshots of two helical mills at full radial immersion with (*a*) 4 flutes, and (*b*) 5 flutes. The snapshots illustrate the top view for an axial slice of the cutter during the beginning, middle, and end of one cutting period.

of flutes results in a constant number of engaged flutes throughout any cutting period. In contrast, an odd number of flutes leads to a situation where the number of engaged teeth is reduced by one at half the cutting period.

Figure 9 explains the change in the number of engaged flutes at full radial immersion for two cutters with opposite parities using a top view of a milling schematic. As an example of a cutter with even parity, Fig. 9(*a*) shows a 4-flute cutter during the beginning, middle, and end of one cutting period. It can be seen that 2 flutes remain engaged throughout the cutting period. The distribution of the even number of flutes ensures that a new flute enters the cut as soon as one of the flutes exits. Similar diagrams can be obtained for 6, 8, or any other even number of flutes. In contrast, Fig. 9(*b*) depicts a 5-flute cutter at full radial immersion. It can be seen that at the beginning of the cut, 3 flutes are engaged simultaneously. However, in the middle of the period, i.e., $\theta = \theta_p/2$ or, equivalently, $t = T/2$, the leading flute exits the cut and only two flutes remain. The change in the number of cutting flutes leads to abrupt changes in the directional force coefficient $K_c(t,b)$ in Eq. (9), causing

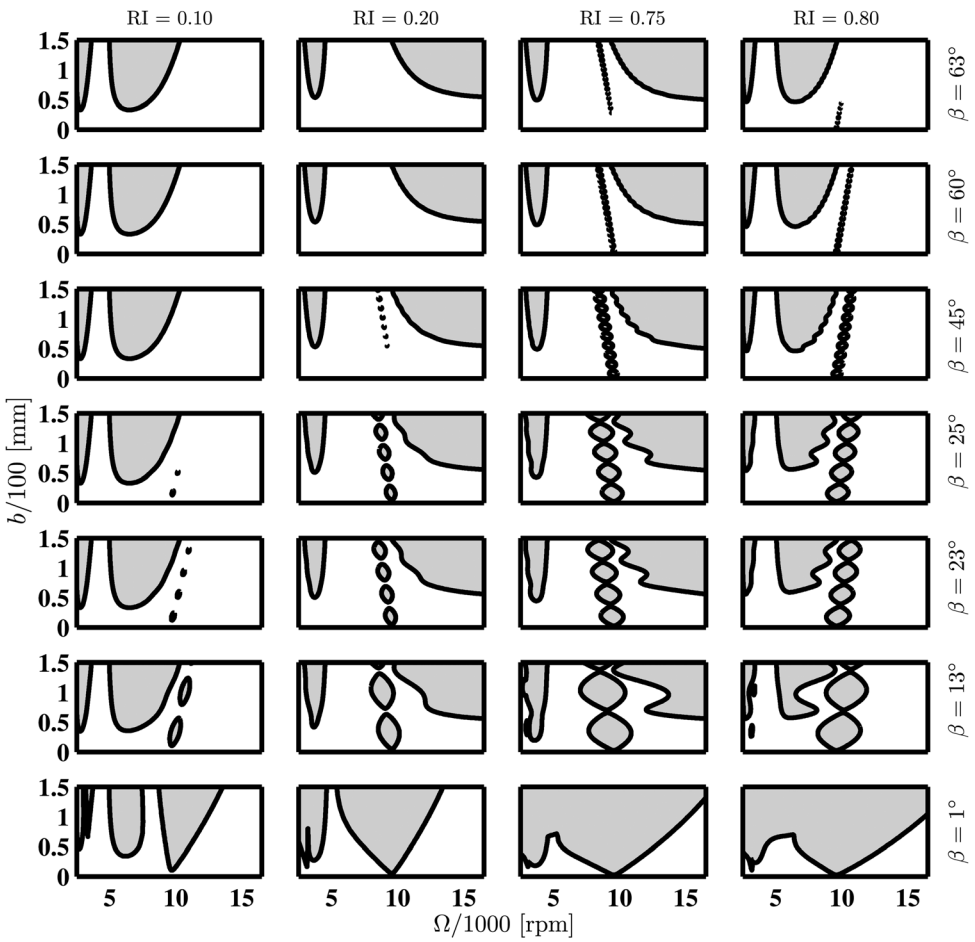

Fig. 10 Upmilling stability charts for the 4 cutting flutes and for the radial immersion values of 0.10, 0.20, 0.75, and 0.80 (columns) and the helix angle values of 1, 13, 23, 25, 45, 60, and 63° (rows)

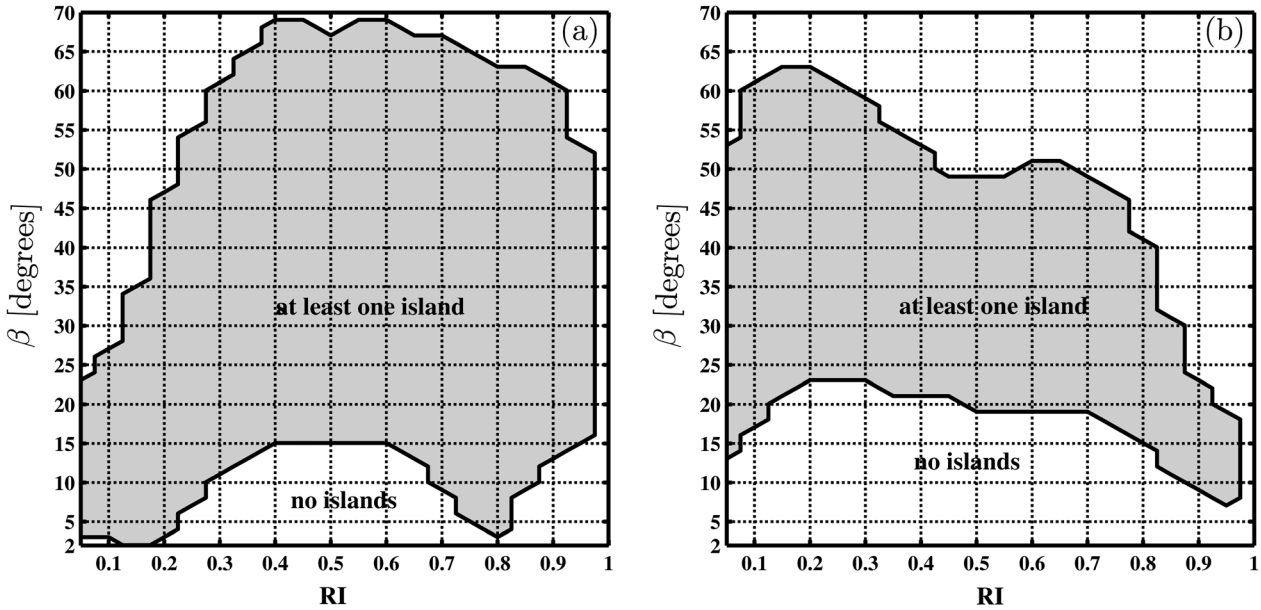

Fig. 11 Diagrams showing the combinations of radial immersion and helix angle where islands occur (shaded region). Results are for 4 cutting flutes and (*a*) upmilling, and (*b*) downmilling.

period-doubling regions to appear [26]. However, as the number of odd cutting flutes is increased, e.g., to 9 in Fig. 8, the helical flutes smooth out these changes and only Hopf lobes appear in the stability chart.

The stability diagrams reported in Figs. 6, 7, and 8 were for a dowmilling model; nevertheless, the stability diagrams of upmilling also demonstrated interesting features, especially when varying the helix angle and the radial immersion. For example, in Fig. 10, a set of stability plots for upmilling with 4 flutes are given for different combinations of radial immersion and helix angle values. The radial immersion values are 0.10, 0.20, 0.75, and 0.80 and vary from left to right, whereas the helix angle values of 1, 13, 23, 25, 45, 60, and 63° vary from the bottom to the top. Therefore, each row corresponds to a constant helix angle while each column corresponds to a constant value of the radial immersion. The values of the helix angle and the radial immersion were chosen to capture the qualitative changes in the upmilling stability plots. Note that the used values of the depth of cut were exaggerated beyond practical limits in order to elucidate the changes in the stability properties of the nonzero helix model.

As the radial immersion and helix angle were varied in Fig. 10, several trends of the changes in the stability properties appeared. For example, when the radial immersion was changed from 0.10 to 0.20 and from 0.75 to 0.80, the change in the mutual orientation of the islands and the secondary Hopf stability lobes was observed. This transition can be explained by the sign change of the cutting force coefficient averaged over one period, as was shown in Refs. [25,26]. This phenomenon was discovered for downmilling in Ref. [25] for a model with compliance in the x direction (see Fig. 2). However, unlike the model in Ref. [25], this analysis used a y compliance model which explains the occurrence of the same phenomenon in upmilling.

By producing more stability charts between $\mathrm{RI} = 0.1$ and $\mathrm{RI} = 0.2$, it can be shown that this transition happens gradually: the major Hopf lobe to the left of the island chain "in the stability diagram for $(\mathrm{RI}, \beta) = (0.1, 13)$ at first completely disappears and then reappears back on the other side of the island chain" while changing its incline to the horizontal axis. Similar transitions happen for other pairs of stability charts, for instance, for $(\mathrm{RI}, \beta) = (0.75, 23)$ and $(0.8, 23)$, except that the mutual orientation of the Hopf lobes and period-doubling islands changes in the opposite direction.

Furthermore, it should be noted that the radial immersions at which the transitions in the stability characteristics occur correspond to the two minima of the lower boundary of the shaded region in Fig. 11(*a*) at the radial immersions approximately equal to 0.15 and 0.8. As the value of the helix angle increases, the sizes and vertical positions of the islands change. The common tendency is that the islands shrink and eventually disappear as β is increased; however, for lower radial immersions this disappearance happens faster, while for higher radial immersions it is slower.

In addition, it is seen that when the islands are to the right of the Hopf lobes, they shrink and disappear while moving downward (see the $\mathrm{RI} = 0.1$ and $\mathrm{RI} = 0.8$ columns in Fig. 10), while in the opposite case they move upward, which is seen in the $\mathrm{RI} = 0.2$ and $\mathrm{RI} = 0.75$ columns. Another observation is that the waviness of the Hopf lobe sections adjacent to the islands is present, especially for higher immersions, and the authors believe that this is a feature that has not been observed in the earlier works on the stability analysis of helical milling tools. The shape of the wavy section of a Hopf lobe changes along with the upward or downward motion of islands as the helix angle is increased. The waviness becomes insignificant once the islands become sufficiently small.

The disappearance and reappearance of the islands in the stability diagrams of both upmilling and downmilling was investigated in Fig. 11 for a 4-flute cutter. Diagrams 11(*a*) and 11(*b*) show at which combinations of radial immersions and helix angles the islands occurred in upmilling and downmilling, respectively. When the combination of radial immersions and helix angles falls into a shaded region, at least one island is present in the corresponding stability chart, while no islands exist for the parameter combinations in the unshaded region. The diagram in Fig. 11(*a*) qualitatively describes the upmilling stability charts in Fig. 10, while Fig. 11(*b*) is added for completeness. The diagrams in Fig. 11 were produced in the grid of radial immersions varying from 0.05 to 1 with the step of 0.05 and the helix angle values varying from 2 to 70 degrees with the step of 2°, and this fact contributed to the coarseness of the plots.

4 Conclusions

This paper investigated the stability of a milling process with simultaneously engaged flutes using the state-space TFEA and Chebyshev collocation methods. In contrast to prior works, multiple flute engagement due to both the high depth of cut and high step-over distance was considered, see Figs. 1(*c*) and 1(*d*).

A particular outcome of this study was the demonstration of different stability behavior in comparison to prior works. To elaborate,

period-doubling regions were shown to appear at relatively high radial immersions when multiple flutes with either a zero or nonzero helix angle were simultaneously cutting. This was shown using a set of stability charts for downmilling that compared a zero-helix mill to a helical tool under the assumption of constant specific cutting coefficients. It was shown that the TFEA and the Chebyshev collocation results agreed with the frequency domain stability results for the low radial immersion cases found in literature (see Figs. 1(*a*) and 1(*b*)). However, in contrast to prior works, period-doubling regions appeared at relatively high radial immersions when multiple flutes were simultaneously cutting.

These regions appeared as lobes for zero-helix tools, while closed islands characterized the period-doubling regions for helical tools. However, as the number of cutting edges was increased, e.g., to 6 and 8 in Fig. 7, the helical flutes smoothed out the force discontinuities and eliminated period-doubling bifurcations. Additionally, in agreement with prior works, period-doubling bifurcations were shown to cease to exist at depths of cut equal to integer multiples of the mill helix pitch.

We also demonstrated stability differences that occur due to the parity in the number of flutes, as shown in Figs. 9 and 7 and 8. In particular, we showed that whereas islands disappeared at full radial immersion for helical cutters with an even parity, cutters with odd parity produced islands even at full radial immersion, as shown in the last row of Fig. 8 for cutters with 3, 5, and 7 flutes. This effect in cutters with odd parity is a result of the abrupt changes in the directional force coefficient as the leading flute starts exiting the cut midway through the period (see Fig. 9). In contrast, at full radial immersion, cutters with even parity maintained a constant number of flutes in the cut throughout the period and only produced Hopf lobes as shown in the last row of Fig. 7.

The study of the stability in upmilling revealed more interesting features for helical mills. For instance, Fig. 10 showed that certain combinations of radial immersion and helix angle gave rise to Hopf lobes with pronounced waviness along the depth of the cut direction. This contrasts with the Hopf lobes usually reported in milling literature and it reflects the strong effect of the helical flutes on the shown cases. Figure 10 also showed the change in the mutual orientation of the islands with respect to the secondary Hopf lobe when varying the helix angle and the radial immersion. This transition was found to gradually occur with increasing the radial immersion where the islands would first shrink slowly, then disappear before they finally reappear on the other side of the Hopf lobe. This transition of the lobes is attributed to the sign change of the cutting force coefficient averaged over one period. Furthermore, we found that the radial immersions at which the transitions in the stability characteristics occurred corresponded to the two minima of the lower boundary of the shaded region in Fig. 11(*a*). Although a similar transition in the stability lobes was demonstrated for zero-helix tools in Refs. [25,26], this study is the first to confirm that a similar transition also occurs for helical tools.

Another observation from Figs. 7, 8, and 10 is the sensitivity of the period-doubling islands to the radial immersion. This sensitivity to the changes in the radial immersion was described qualitatively in Fig. 11 for both upmilling and downmilling. It was shown that even small changes of the radial immersion can cause the islands to disappear (or reappear) in the stability diagrams. Figure 11 also reiterates the prior conclusion that no period-doubling regions appear for cutters with an even number of flutes.

Finally, although only Hopf and period-doubling bifurcations can occur for tools with constant helix angle and constant pitch, a recent study has found cyclic-fold bifurcations at low radial immersions for both variable pitch and variable helix tools [45]. However, expanding the approach of this paper to the cases of variable pitch and variable helix tools remains a topic for future research.

Acknowledgment

Support from the U.S. National Science Foundation with Grant Nos. CMMI-0900289 and CMMI-0900266 is gratefully acknowledged.

References

[1] Stépán, G., 1989, *Retarded Dynamical Systems: Stability and Characteristic Functions*, John Wiley & Sons, New York.
[2] Insperger, T., and Stépán, G., 2004, "Updated Semi-Discretization Method for Periodic Delay-Differential Equations With Discrete Delay," Int. J. Numer. Methods Eng., **61**, pp. 117–141.
[3] Ma, H. Butcher, E. A., and Bueler, E., 2003, "Chebyshev Expansion of Linear and Piecewise Linear Dynamic Systems With Time Delay and Periodic Coefficients Under Control Excitations," ASME J. Dyn. Syst., Meas., Control, **125**, pp. 236–243.
[4] Butcher, E., Ma, H., Bueler, E., Averina, V., and Szabó, Z., 2004, "Stability of Linear Time-Periodic Delay-Differential Equations Via Chebyshev Polynomials," Int. J. Numer Methods Eng., **59**, pp. 895–922.
[5] Deshmukh, V., Ma, H., and Butcher, E. A., 2006, "Optimal Control of Parametrically Excited Linear Delay Differential Systems Via Chebyshev Polynomials," Opt. Control Appl. Methods, **27**, pp. 123–136.
[6] Engelborghs, K., Luzyanina, T., 'T. Hout, K. J., and Roose, D., 2000, "Collocation Methods for the Computation of Periodic Solutions of Delay Differential Equations," SIAM J. Sci. Comput. (USA), **22**, pp. 1593–1609.
[7] Argyris, J. H., and Scharpf, D. W., 1969, "Finite Elements in Time and Space," Nucl. Eng. Des., **10**(4), pp. 456–464.
[8] Borri, M., Bottasso, C., and Mantegazza, P., 1992 "Basic Features of the Time Finite Element Approach for Dynamics," Meccanica, **27**, pp. 119–130.
[9] Mann, B. P., Garg, N. K., Young, K. A., and Helvey, A. M., 2005, "Milling Bifurcations from Structural Asymmetry and Nonlinear Regeneration," Nonlinear Dyn., **42**, pp. 319–337.
[10] Patel, B. R., Mann, B. P., and Young, K. A., 2008, "Uncharted Islands of Chatter Instability in Milling," Int. J. Mach. Tools Manuf., **48**, pp. 124–134.
[11] Budak, E., and Altintaş, Y., 1998, "Analytical Prediction of Chatter Stability Conditions for Multi-Degree of Systems In Milling. Part I: Modelling," ASME J. Dyn. Syst., Meas., Control, **120**(1), pp. 22–30.
[12] Merdol, S., and Altintas, Y., 2004, "Multi Frequency Solution of Chatter Stability for Low Immersion Milling," ASME J. Manuf. Sci. Eng., **126**(3), pp. 459–466.
[13] Schmitz, T. L., Davies, M. A., Medicus, K., and Snyder, J., 2001, "Improving High-Speed Machining Material Removal Rates by Rapid Dynamic Analysis," CIRP Ann., **50**(1), pp. 263–268.
[14] Smith, S., and Tlusty, J., 1991 "An Overview of the Modeling and Simulation of the Milling Process," ASME J. Eng. Ind., **113**, pp. 169–175.
[15] Montgomery, D., and Altintaş, Y., 1991, "Mechanism of Cutting Force and Surface Generation in Dynamic Milling," ASME J. of Eng. Ind., **113**, pp. 160–168.
[16] Zhao, M. X., and Balachandran, B., 2001, "Dynamics and Stability of Milling Process," Int. J. Solids Struct., **38**(10–13), pp. 2233–2248.
[17] Altintaş, Y., and Budak, E., 1995 "Analytical Prediction of Stability Lobes in Milling," CIRP Ann., **44**(1), pp. 357–362.
[18] Davies, M. A., Pratt, J. R., Dutterer, B., and Burns, T. J., 2002, "Stability Prediction for Low Radial Immersion Milling," ASME J. Manuf. Sci. Eng., **124**(2), pp. 217–225.
[19] Minis, I., and Yanushevsky, R., 1993, "A New Theoretical Approach for Prediction of Machine Tool Chatter in Milling," ASME J. Eng. Ind., **115**, pp. 1–8.
[20] Insperger, T., and Stépán, G., 2000, "Stability of the Milling Process," Period. Polytech., **44**(1), pp. 47–57.
[21] Mann, B. P., Bayly, P. V., Davies, M. A., and Halley, J. E., 2004, "Limit Cycles, Bifurcations, and Accuracy of the Milling Process," J. Sound Vib., **277**, pp. 31–48.
[22] Insperger, T., Mann, B. P., Stépán, G., and Bayly, P. V., 2003," Stability of Up-Milling and Down-Milling, Part 1: Alternative Analytical Methods," Int. J. Mach. Tools Manuf., **43**, pp. 25–34.
[23] Mann, B. P., Young, K. A., Schmitz, T. L., and Dilley, D. N., 2005, "Simultaneous Stability and Surface Location Error Predictions in Milling," ASME J. Manuf. Sci. Eng., **127**, pp. 446–453.
[24] Schmitz, T. L., and Mann, B., 2006, "Closed Form Solutions for the Prediction of Surface Location Error in Milling," Int. J. Mach. Tools Manuf., **46**, pp. 1369–1377.
[25] Butcher, E., Bobrenkov, O., Bueler, E., and Nindujarla, P., 2009, "Analysis of Milling Stability by the Chebyshev Collocation Method: Algorithm and Optimal Stable Immersion Levels," ASME J. Comput. Nonlinear Dyn., **4**(3), p. 031003.
[26] Bobrenkov, O., Khasawneh, F., Butcher, E., and Mann, B., 2010, "Analysis of Milling Dynamics for Simultaneously Engaged Cutting Teeth," J. Sound Vib., **329**(5), pp. 585–606.
[27] Tobias, S. A., 1965, *Machine Tool Vibration*, Blackie, London.
[28] Tlusty, J., and Polacek, M., 1963, "The Stability of Machine Tools Against Self-Excited Vibrations in Machining," *Proceedings of the ASME International Research in Production Engineering*, Pittsburgh, PA, pp. 465–474.
[29] Merrit, H. E., 1965, "Theory of Self-Excited Machine-Tool Chatter," ASME J. Eng. Ind., **87**(4), pp. 447–454.
[30] Davies, M., Pratt, J., Dutterer, B., and Burns, T., 2000, "The Stability of Low Radial Immersion Milling," CIRP Ann., **49**(1), pp. 37–40.
[31] Bayly, P. V., Halley, J. E., Mann, B. P., and Davis, M. A., 2003, "Stability of Interrupted Cutting by Temporal Finite Element Analysis," ASME J. Manuf. Sci. Eng., **125**, May, pp. 220–225.
[32] Insperger, T., Stépán, G., Bayly, P. V., and Mann, B. P., 2003, "Multiple Chatter Frequencies in Milling Processes," J. Sound Vib., **262**, pp. 333–345.
[33] Mann, B. P., Insperger, T., Bayly, P. V., and Stépán, G., 2003, "Stability of Up-Milling and Down-Milling, Part 2: Experimental Verification," Int. J. Mach. Tools Manuf., **43**(1), pp. 35–40.

[34] Balachandran, B., 2001, "Non-Linear Dynamics of Milling Process," Proc. R. Soc. London, Ser. A, **359**(1781), pp. 793–819.
[35] Insperger, T., Muñoa, J., Zatarain, M., and Peigné, G., 2006, "Unstable Islands in the Stability Chart of Milling Processes Due to the Helix Angle," *Proceedings of CIRP Second International Conference on High Performance Cutting*, June 12 and 13, CIRP, Vancouver, Canada.
[36] Zatarain, M., Muñoa, J., Peigné, G., and Insperger, T., 2006, "Analysis of the Influence of Mill Helix Angle on Chatter Stability," CIRP Ann., **55**, pp. 1–4.
[37] Mann, B., Edes, B., Easley, S., Young, K., and Ma, K., 2008, "Chatter Vibration and Surface Location Error Prediction for Helical End Mills," Int. J. Mach. Tools Manuf., **48**, pp. 350–361.
[38] Altintaş, Y., 2000, *Manufacturing Automation*, 1st ed., Cambridge University Press, New York.
[39] Martelloti, M. E., 1941, "An Analysis of the Milling Process," Trans. ASME, **63**, pp. 677–700.
[40] Martelloti, M., 1945, "An Analysis of the Milling Process, Part 2: Down-milling," Trans. ASME, **67**, pp. 233–251.
[41] Mann, B., and Patel, B., 2010, "Stability of Delay Equations Written as State Space Models," J. Vib. Control, **16**, pp. 1067–1085.
[42] Khasawneh, F., Mann, B., Bobrenkov, O., and Butcher, E., 2009, "Self–Excited Vibrations in a Delay Oscillator: Application to Milling With Simultaneously Engaged Helical Flutes," *Proceedings of the ASME 2009 International Design Engineering Technical Conferences & Computers and Information in Engineering Conference*, August 30-September 2, 2009, San Diego, California, paper no. DETC2009-86636.
[43] Khasawneh, F., Patel, B., and Mann, B., 2009, "A State-Space Temporal Finite Element Approach for Stability Investigations of Delay Equations," *Proceedings of the ASME 2009 Conference on Smart Materials, Adaptive Structures and Intelligent Systems*, September 21–23, 2009, Oxnard, California, paper no. SMASIS2009-1263.
[44] Szalai, R., and Stépán, G., 2006, "Lobes and Lenses in the Stability Chart of Interrupted Turning," ASME J. Comput. Nonlinear Dyn., **1**, pp. 205–211.
[45] Sims, N. D., Mann, B., and Huyanan, S., 2008, "Analytical Prediction of Chatter Stability For Variable Pitch and Variable Helix Milling Tools," J. Sound Vib., **317**, pp. 664–686.